H-Bonding Supramolecular Assemblies of PTCDI Molecules on the Au(111) Surface

M. Mura,[†] F. Silly,[‡,§,||] G. A. D. Briggs,[||] M. R. Castell,[||] and L. N. Kantorovich*,[†]

Physics, King's College London, The Strand, London, WC2R 2LS, United Kingdom; CEA, IRAMIS, SPCSI, Nanostructures and Organic Semiconductors, F-91191 Gif-sur-Yvette, France; UPMC, IPCM, UMR CNRS 7201, 4 place Jussieu, 75005 Paris, France; and Department of Materials, University of Oxford, Parks Road, Oxford OX1 3PH, United Kingdom

Using a combination of scanning tunneling microscopy (STM) in ultrahigh vacuum (UHV) and a systematic theoretical method based on considering all possible hydrogen bond connections between molecules with subsequent density functional theory (DFT) calculations, we studied supramolecular assemblies of highly symmetrical rectangular PTCDI molecules on the Au(111) surface. We show, using a systematic prediction procedure followed by ab initio density functional calculations, that just over 10 monolayer structures are possible assuming two molecules in the primitive cell, some of which would appear indistinguishable in the STM images. By breaking down these structures into distinct assemblies, we predict six possible phases. Two of these had been observed previously: a canted phase seen on a number of surfaces including Au(111) and a brick wall phase seen so far only on the NaCl(001) surface. Using STM imaging of PTCDI molecules on the Au(111) surface in ultrahigh vacuum, we discovered a completely new "domino" phase, also predicted by our theory, in which molecules attach to each other rather like dominoes, to form squares repeated periodically across the surface. The interaction of the molecules with the gold surface seems to influence the orientation of the phases but not necessarily their stability.

I. Introduction

Many organic molecules are known to have the ability to self-assemble in two-dimensional networks when they are deposited on inorganic (e.g., metallic) surfaces, which has been of considerable interest recently.[1–4] In particular, an emerging possibility for these structures to form either chiral or nonchiral ordered structures[5,6] has been intensively studied in view of possible applications in nanotechnology (e.g., refs 1 and 7).

Perylene-3,4,9,10-tetracarboxylic-3,4,9,10-dianhydride (PTCDA) and perylenetetracarboxylic diimine (PTCDI) molecules are of special interest in engineering of two-dimensional (2D) porous nanostructures due to their special rectangular shape (see Figure 1) and a specific hydrogen-bonding functionality near the edges. These long molecules have been employed, alone or combined with other molecules such as melamine, as building blocks for engineering sophisticated multicomponent supramolecular architectures, or templates, capable of trapping foreign molecules (e.g., fullerenes[1,3,8–10]).

From an experimental point of view, only supramolecular assemblies of PTCDA molecules have been intensively studied on different surfaces (see, e.g. refs 8 and 11–25), and a number of different phases have been identified. However, much less attention has been devoted to the PTCDI molecules. As far as we are aware, these molecules were deposited on the graphite and MoS$_2$[11], Ag/Pt(111),[26] Pt(100),[27] NaCl(001),[28] Au(111),[29,30] and Ag/Si(111)[8] surfaces, and basically two structures have been reported: a canted and a brick wall one. In the canted structure the molecules within and between rows are connected by their
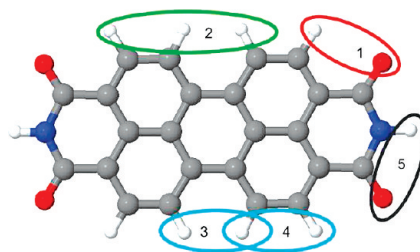

Figure 1. PTCDI molecule and its nonequivalent binding sites shown by numbered ovals.

edges.[8,11,29,30] The rows of the canted structure have also been observed separately as chains.[8,31] In the brick wall phase[28] the molecules are oriented along the rows, and the adjacent rows are shifted with respect to each other. It is surprising that more PTCDI phases have not been observed, especially since PTCDI molecules have the ability to form stronger hydrogen bonds with each other as compared to their PTCDA counterparts.

In this paper we apply scanning tunneling microscopy (STM)[32,33] to perform a detailed study of self-assembled structures formed by PTCDI molecules on the Au(111) surface after deposition at room temperature in ultrahigh vacuum (UHV) conditions. Three different structures have been found, one of which has never been previously reported, while the other was only reported on the NaCl(001) surface. The experimental data are supported by extensive theoretical analysis. In order to consider all possible structures the PTCDI molecules can form, we use a systematic approach developed earlier for adenine[34] and used in the previous studies of melamine[35] and PTCDA.[24] Due to the high symmetry of the molecules, the number of dimers and, therefore, two-dimensional assemblies they can form will be shown to be limited. These findings are in concert with the relatively small number of two-dimensional

* To whom correspondence should be addressed. E-mail: lev.kantorovitch@kcl.ac.uk. Tel: +44(0)2078482160. Fax: +44(0)2078482420.
† King's College London.
‡ Nanostructures and Organic Semiconductors.
§ UMR CNRS 7201.
|| University of Oxford.

PTCDI Molecules on the Au(111) Surface

J. Phys. Chem. C, Vol. 113, No. 52, 2009 **21841**

structures found for other symmetric molecules such as melamine[35] and PTCDA;[24] at the same time, they are contrasted by a very large number of assemblies found for the adenine molecule which does not have any point symmetry.[34]

The plan of this paper is as follows. In section II we briefly outline the experimental and theoretical methods used. PTCDI self-assembled monolayers observed in this study in STM experiments are described in section III, while the corresponding theoretical analysis is performed in section IV. Finally, a short discussion and conclusions are given in section V.

II. Methods

A. Experimental Section. Au(111) films grown on mica were used as a substrate. The samples were introduced into the ultrahigh vacuum (UHV) chamber of an STM (JEOL JSTM4500S) operating at a pressure of 10^{-8} Pa. Samples sputtered with argon ions with subsequent annealing in UHV at temperatures between 600 and 800 °C, typically for 30 min, were used to prepare the gold surface. PTCDI molecules were sublimated at 335 °C and then deposited on the surface which was kept at room temperature. The deposition flux was 1−2 monolayers per hour. The sample was not postannealed after molecular deposition. Etched tungsten tips were used to obtain constant current images at room temperature with a bias voltage applied to the sample. STM images have been processed and analyzed using the homemade FabViewer application.[36]

B. Theoretical. To construct all possible structures, a systematic approach was used as described, e.g., in refs 34 and 35. It consists of the following steps: (i) identification of all binding sites the molecule has on its periphery; only such sites are considered that can participate in hydrogen bonding with another molecule; other possible sites are considered nonfunctional and subsequently ignored; (ii) construction of all dimers; (iii) using dimer rules, connect the molecules; all possible unit cells are constructed having a predefined number of molecules; (iv) then for every unit cell found all possible chains (i.e., one-dimensional structures) are built; (v) by attaching chains parallel to each other, all possible 2D periodic structures are formed with their stabilities estimated by summing up all dimer energies (per cell). Finally, the most stable predicted structures are fully relaxed using an ab initio method to obtain their geometries and binding energies.

The calculations were performed using the ab initio SIESTA method,[37,38] which is based on a localized numerical orbital basis set, periodic boundary conditions, and the first principles scalar-relativistic norm-conserving Troullier−Martins[39] pseudopotential factorized in the Kleinman−Bylander[40] form. We used the Perdew, Becke, and Ernzerhof (PBE)[41] generalized gradient approximation for the exchange and correlation which was found previously to be adequate in representing hydrogen bonding between DNA base molecules.[42] In each calculation, atomic relaxation was performed until forces on atoms were less than 0.01 eV/Å in the cases of dimers and 0.03 eV/Å in the cases of monolayers.

To analyze the constructed assemblies, we used several energies.[24,35,43,44] The overall stability is determined by the stabilization energy, E_{stab}, defined as the total energy of the relaxed combined system (e.g., the PTCDI dimer) minus the total energies of all its individual components (two PTCDI molecules) relaxed separately. For stable systems $E_{stab} < 0$. To characterize the interaction between the two parts of a composite system (e.g., a pair), the interaction energy, E_{int}, is used; it is defined as the energy of the whole system minus the energy of each individual

molecule calculated in the geometry of the relaxed combined system. It is always negative for a stable system. Finally, the (always positive) deformation energy, E_{def}, characterizes energies lost by each part of the combined system (e.g., the two molecules of the pair) due to their subsequent relaxation from their stable geometry at infinity.

Since the interaction and deformation energies, as defined above, sum up exactly to the stabilization energy, $E_{stab} = E_{int} + E_{def}$, for a stable structure the loss due to deformation (positive) must be compensated by the interaction energy (negative). Note, however, that since we use SIESTA, which employs a localized basis set, the basis set superposition error (BSSE) correction must be applied to correct the final stabilization energies. The counterpoise correction method due to Boys and Bernardi[45] has been used here for that purpose. To simplify the analysis, the same BSSE correction was also applied to the interaction energy ensuring that the mentioned exact relationship is still valid for the final energies.

The stabilization energy gives an overall stability of a hydrogen bonded system. To assess the stability of individual hydrogen bonds, one might look at the geometry of the donor−H−acceptor group of atoms:[34,42] in strong hydrogen bonds these three atoms accept the geometry close to linear with the two distances to the H atom being of the order of 2.6−2.8 Å. To characterize the strength of the hydrogen bonds in a system, the electron density difference was also found to be extremely helpful:[24,34,35,42,44,46,47] hydrogen bonds display a so-called "kebab" structure of alternating regions of charge excess and depletion. The stronger the bond, the more "regular" the kebab structure is. This concept is quite general, and this kind of analysis will be heavily used in this study.

Our DFT calculations were performed without taking account of the interaction with the surface, i.e., in the "gas phase". This method is appropriate for the Au(111) surface we are concerned with here, at least as the first approximation, since the molecule−surface interaction has very little corrugation across the surface.[48] It was found in these calculations that for a similar PTCDA molecule adsorbed on the Au(111) surface, there is no noticeable charge transfer between the molecule and the surface since all occupied states of the molecule fall below the Fermi level of the gold, and the dispersion interaction is the main binding mechanism. Moreover, it was also found that the variation of the adsorption energy across the surface corresponds to about 2% of the adsorption energy itself.

III. Supramolecular Assemblies of PTCDI Molecules: STM Observations

After deposition of the PTCDI molecules on the Au(111) surface, large terraces covered with the assemblies of the molecules were seen. Upon careful analysis, three different phases were identified as shown in Figure 2. In the first phase, Figure 2a, we see rows of canted molecules running parallel to each other. The PTCDI rows are aligned in the [11$\bar{2}$] gold direction, in agreement with ref 30. Molecules in every other row are tilted in the same direction at an angle which is approximately 12° to the row direction. The shapes of the molecules in the rows between these ones are not well resolved. However, there are indications that these are tilted in the opposite direction by the same angle of 12°. We believe that this is a canted structure already observed on the Au(111) and Ag/Si(111) surfaces previously.[8,29,30]

The next structure we saw, shown in Figure 2b, has never been reported before. In this "domino" structure the molecules are arranged in what can be approximately seen as squares; each
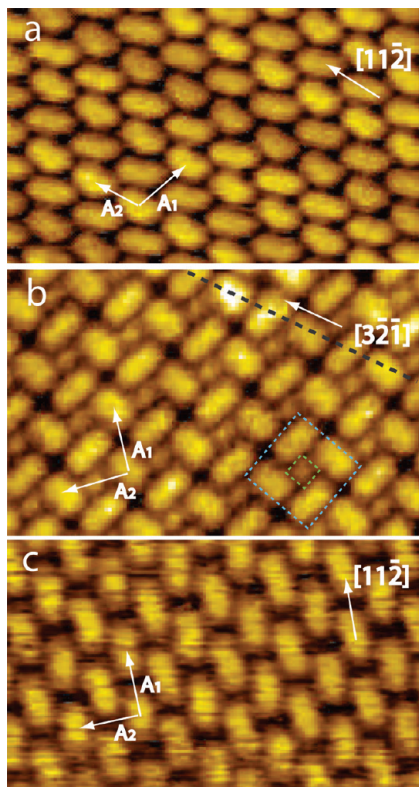
Figure 2. Three PTCDI monolayers observed with STM on the Au(111) surface (10 × 7 nm²): canted (a), domino (b), and brick wall (c) structures. In each case the alignment direction of one of the rows of the molecules with respect to the gold surface is explicitly indicated. The lattice vectors are indicated by white vectors in each case. Tunneling parameters: (a, b) $I_t = 0.1$ nA, $V_s = -1.8$ V; (c) $I_t = 0.5$ nA, $V_s = -1.8$ V. A black dotted line in (b) indicates a row of molecules aligned along the [32$\bar{1}$] gold direction.

square is made out of four molecules attached to each other as domino pieces. Rows of molecules are aligned in the [32$\bar{1}$] gold direction. Two different types of squares delimited by the PTCDI molecules can be seen with different contrast in their centers. Larger squares appear brighter than the smaller ones. We believe that this effect can be attributed merely to the sizes of the two gaps created by the molecules: the larger square gaps are big enough for the gold surface electronic states to protrude sufficiently resulting in an increase of the local density of states (DOS). At the same time, the gold states are pushed out by the molecular states within the smaller gaps, so that a local decrease of the DOS is expected. In order to check this hypothesis, one would have to perform a local DOS calculation for this monolayer adsorbed on the gold surface. Since both structures are incommensurable and the PTCDI monolayer unit cell is quite large, this kind of calculation would be impossible to do at present. Experimentally, similar a phenomenon has been observed in a melamine network on the Au(111) surface, where the signal in the center of the melamine hexagons appears lower in contrast to the signal due to the clean gold surface in the STM images; see Figure 3 in ref 44.

In the structure seen in Figure 2c molecules are arranged in identical rows shifted with respect to each other; molecules within the rows are aligned along the [11$\bar{2}$] direction of the gold surface. This arrangement is equivalent to the brick wall structure formed by PTCDA molecules on a number of substrates[18,23] and was previously observed to be formed by PTCDI molecules only on the NaCl(001) surface.[28]

The observed lengths of the lattice vectors and the angle between them γ (in degrees) for the three structures were

measured to be (a) canted: $A_1 = 16.7$ Å (nearly perpendicular to the row direction), $A_2 = 13.7$ Å (along the direction of the canted rows), $\gamma = 100°$; (b) domino: $A_1 = 17.9$ Å, $A_2 = 17.0$ Å, $\gamma = 95°$, and (c) brick wall: $A_1 = 18.7$ Å, $A_2 = 17.0$ Å, $\gamma = 90°$. Note that the lattice vector A_1 observed in this study is slightly different from that measured previously for the same system in ref 30. At the same time, the lattice vector A_2 along the canted rows is very close to that in the previous measurements. This must indicate that the interaction between the molecules *within* the canted rows is much stronger than that *between* the rows. This suggests that different PTCDI−PTCDI lateral packing may occur.

STM images showed that the canted structure was the prevailing PTCDI network covering the gold surface. The brick wall and domino structures were only observed locally. The size of the molecular networks was usually larger than 25 × 25 nm².

IV. Supramolecular Assemblies of PTCDI Molecules: Theoretical Analysis

A. PTCDI Structures in the Gas Phase. The structure of the PTCDI molecule is close to that of the PTCDA: instead of the central oxygen atom at short sides of it there is an imide group; see Figure 1. This small change in the molecule design leads, as we shall see, to essential differences in structures these molecules can form with each other. Although some of the structures are similar to those formed by PTCDA,[24] there are also very different monolayers possible which are entirely due to an ability of the PTCDI molecules form dimers which are unique to them.

In this section we shall consider all possible gas-phase structures based on two PTCDI molecules in the unit cell. We will describe in detail the approach used presenting first the PTCDI dimers; this will be followed by building all superstructures based on the dimer unit cells.

1. PTCDI Dimers. Again, we start by identifying the binding sites of the PTCDI molecule; see Figure 1. Five possible types of binding sites can be identified, where three of them are exclusively donors (sites 2, 3, and 4) composed of carbon−hydrogen groups and are able to form double or triple hydrogen bonds with sites presenting acceptor atoms. In the case of PTCDI, such purely acceptor sites do not exist (but they exist in the case of PTCDA[24]), so that sites 2, 3, and 4 cannot be functional. However, as we shall see in the following, two of the possible dimers do involve these sites to some extent. The two other types of binding sites have both donor and acceptor atoms (sites 1 and 5) composed of oxygen and hydrogen atoms which are able to form a double hydrogen bond with a binding site of the same type (reversed). There are four binding sites 1 and the same number of binding sites 5 around the molecule perimeter.

Combining binding sites 1 and 5, it is possible to obtain three pairs, D1, D2, and D3, DFT relaxed structures of which are shown in Figure 3, while their energies are reported in Table 1. In each case the dimers are stabilized by two hydrogen bonds. We also find that two other pairs are stable, D4 and D5, shown in Figure 3. We tried these inspired by some experimental observations.[49] In these two pairs purely hydrogen sites (2, 3, and 4) are also somewhat employed.

The most stable dimer is D3, and it is stabilized by a double hydrogen bond between the imine groups of the two PTCDI molecules. The two PTCDI molecules are connected in a "head-and-tail" structure. The dimer D1 is similar to the dimer D3 of PTCDA;[24] however, the stabilization energy in the case of

PTCDI Molecules on the Au(111) Surface
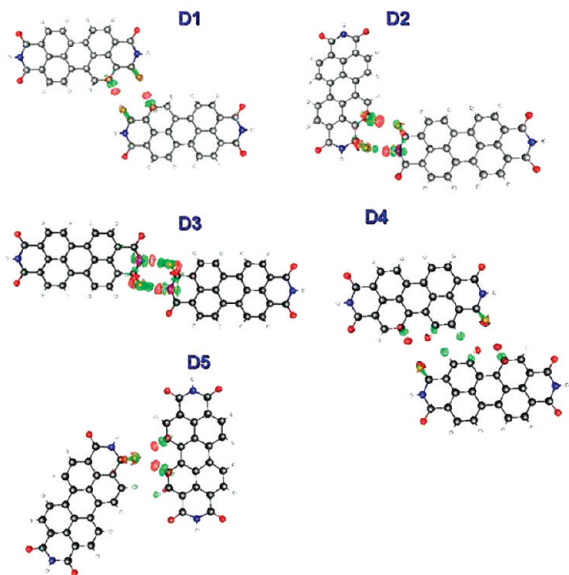
J. Phys. Chem. C, Vol. 113, No. 52, 2009 **21843**

Figure 3. Relaxed geometries of the PTCDI dimers shown together with the corresponding electron density difference plots corresponding to ±0.01 Å^{-3}. The green surfaces correspond to the regions of positive electron difference (excess), and the red areas correspond to the regions of negative electrons density difference (depletion).

TABLE 1: Stabilization Energies (eV) of the PTCDI Dimers^a

index	D1	D2	D3	D4	D5
E_{stab}	−0.15	−0.24	−0.5	−0.11	−0.14
E_{def}	0.05	0.07	0.11	0.03	0.01
E_{int}	−0.20	−0.31	−0.61	−0.14	−0.15
E_{BSSE}	0.14	0.14	0.15	0.12	0.09

^{a} The stabilization and interaction energies include the BSSE correction which is also shown.

PTCDI is lower. This difference in energies is attributed to the difference in the electronic structure of the two molecules. The dimer D2 has an L-shape; it has a much lower stability because one of the hydrogen bonds (out of the two, see Figure 3) is formed by the C−H group of one molecule with the oxygen of another. Very weak dimers D4 and D5 are stabilized by hydrogen bonds formed between the oxygen atoms of the two PTCDI molecules and the hydrogens along the long side of the molecules. Interestingly, the dimer D5 is stabilized only through a little bit more than a single hydrogen bond (see Figure 3) and has a stabilization energy close to that of D1. Recall that the dimers D4 and D5 have been identified in some of the experimental images.[49] As in the case of PTCDA,[24] when carbon atoms are involved in the hydrogen bonding (D1, D2, and D5 dimers), the stabilization energies are very small and the dimers are weak. Deformation energies in all cases are very small.

Once all the possible dimers are constructed, the next step is to identify the binding sites available to connect the PTCDI dimers with each other in such a way so that a 1D chain is obtained. In the next section we present the chains based on the most stable PTCDI pairs, D1, D2, and D3.

2. One-Dimensional Chains Based on the PTCDI Pairs. In this subsection we shall present the 1D structures that can be built using the PTCDI dimer as a unit cell. As before, we start by identifying the binding sites available on the periphery of the dimer (see Figure 3) which are available for the connection with more dimers. We build the 1D chains by connecting dimers in a chainlike manner along one direction. The chains are obtained by adding a second dimer to a certain

binding site of the first dimer, and then a third dimer is added to the same site of the second one, and so on. In this way, using the available dimer binding sites, 16 different chains can be constructed which can be classified into families of "similar" chains, based on considering the evaluated energy (via summing up dimer energies) and the geometry of each chain. Following this procedure, six families of PTCDI chains have been constructed; see Figure 4.

We present here, with a single exception, only the evaluated stabilization energies, based on the sum of the corresponding dimer energies, without performing an additional relaxation of the structures using the DFT method. This is because we find in the case of PTCDA chains that the evaluated and DFT calculated stabilization energies of the chains are very close.[24] In the PTCDI case the same behavior is expected.

As might be expected, the weakest chain is F3 that involves one of the weakest dimer contacts D1, while the most stable chain is F4 that involves by far the strongest dimer D3; see Table 2. One particular chain from this family, F4a, was observed on the Ag terminated Si(111) surface,[8] and that is why we relaxed this chain with our DFT method. A favorable agreement of its geometry can be found with the one observed in ref 8, as is evidenced from Table 3. The binding energy for the chain (per two molecules) was found to be −1.12 eV (the BSSE correction 0.34 eV), which is only slightly higher than the evaluated energy of −1.0 eV reported in Table 2. We expect the strength of the F4b chain to be similar or even identical to that of F4a.

3. Monolayers Based on the PTCDI Dimers. To build all possible 2D structures involving the PTCDI molecules, we followed the same procedure as used in the cases of melamine[35] and PTCDA.[24] Although there are 16 1D chains possible (see subsection IV.A.2) based on the strongest dimers D1, D2, and D3 considered above, only 11 2D structures can be constructed with two molecules in the unit cell using the same dimer connections due to high symmetry of the molecule. Once the monolayer energies are evaluated, it is possible to classify the structures into families of "similar" structures taking into account the geometries and the evaluated energies. In this way, seven families of monolayers can be identified, and one representative from each was considered as a prototype. The selected seven monolayers are shown in Figure 5, and their energies are given in Table 4 while the geometrical characteristics of the unit cells are given in Table 5. One more monolayer MON8 based on the D4 and D5 dimers (or the chain F4a) was considered separately. The MON5 and MON7 monolayers, strictly speaking, contain just one molecule in the primitive unit cell. However, to simplify our discussion, we shall refer to them as containing two molecules, i.e., the corresponding supercells (as defined in Figure 5) will be considered as an elementary unit.

The structure MON2 is similar to the domino structure shown in Figure 2b. The structure MON1 is of a similar nature, albeit more porous, and we shall use the same "domino" name for it. The structures MON3 and MON4 represent two variants of the herringbone phase, with the MON3 monolayer containing elongated pores between molecules, while MON4 is more compact. In the MON5 structure we recognize the brick wall phase observed in our STM images and shown in Figure 2c. MON6 is a somewhat similar phase with large pores formed by six molecules, and we coined the name "porous" for it. In MON7 molecules in each horizontal row go in a wavelike manner, so that we shall call this monolayer "waveform". Finally, MON8 must be the canted structure seen previously[8,29,30] and in this work; see Figure 2a.
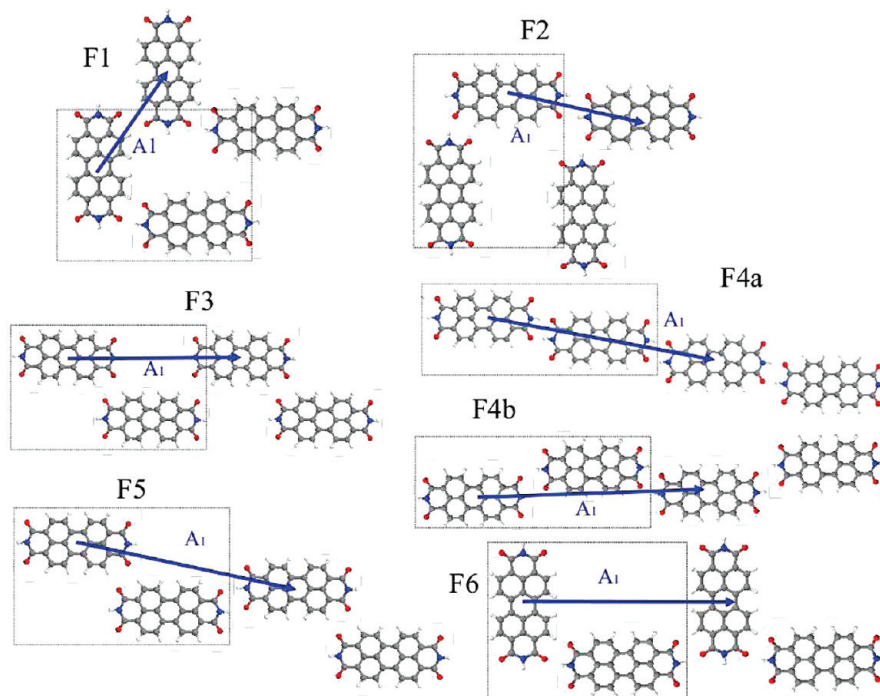
Figure 4. Predicted structures for the selected six PTCDI chains with two unit cells shown explicitly. To facilitate comparison with available experimental data, two chains from the same family F4 are shown here, designated as F4a and F4b. The structure of the F4a chain shown is the only one obtained after the full DFT relaxation. The lattice vector, A_1, and the unit cell, corresponding in all cases to two molecules, are indicated. (Note that, strictly speaking, the periodicity of the chain F4a corresponds to a single molecule in the cell.)

TABLE 2: Evaluated (by Summing Corresponding Dimer Energies) Stabilization Energies (in eV) for Selected PTCDI Chains[a]

index	F1	F2	F3	F4	F5	F6
E_{stab} (eval.)	−0.39	−0.74	−0.30	−1.00	−0.65	−0.48

[a] In all cases the reported energy was calculated per two molecules in the cell.

TABLE 3: Comparison of the Geometrical Characteristics of the (Canted) F4a Chain (with One Molecule in the Unit Cell), Relaxed with Our DFT Method, with the One Observed by STM on the Ag/Si(111) Surface[8] [a]

	STM[8]	this work (DFT)
A_1	14.1 ± 0.2	14.52
β	8 ± 2	10.4

[a] A_1 is the length (in Å) of the lattice vector (i.e., the distance between the molecules), and β (in deg) is the canting angle (the angle molecules make with the direction of the chain).

The most stable PTCDI monolayer is the canted structure MON8 (see Table 4) based on the most stable chain F4a from the previous subsection. Moreover, this monolayer is also more stable than any of the PTCDA monolayers we have considered in ref 24, which is not surprising since PTCDI molecules form one dimer (D3) which is by far more stable than any of the PTCDA dimers. The calculated canted angle (see the previous subsection) along the F4a rows in the relaxed structure $\beta = 11.5°$, which is close the value of 10.4° found for the isolated F4a row in the previous subsection; see Table 3. In the present case the evaluated stabilization energies of monolayers are all smaller than the DFT calculated energies indicating on the existence of cooperative effects.

The difference electron density plots for six of the calculated monolayers are shown in Figure 6. One can see the formation of hydrogen bonds of various strength between the molecules.

The monolayer MON8 (the canted phase) demonstrates well developed hydrogen bonds along the F4a chains. In spite of the fact that the chains themselves are bound together by the not-the-strongest D5 dimer connections (see Table 1), this monolayer is the strongest due to favorable positioning of the molecules so that their binding along the chains is not severely affected. At the same time, a relatively weak binding between the rows may indicate some flexibility in the relative positions of the nearest rows affecting the length of the lattice vector A_1 (which is nearly perpendicular to the direction of the canted rows) and the angle γ it makes with the other lattice vector. The MON7 monolayer also demonstrates quite developed "kebab" structures along the chains; however, fewer hydrogen bonds between the chains (made of relatively weak D1 dimer connections, Table 1) yield this monolayer to be only the next to the strongest one. This monolayer is then followed in energy by MON2 (the domino phase) in which each molecule is connected to four others via the D2 connection of intermediate strength. The other domino phase MON1 and the herringbone phase structures MON3 and MON4, as well as the brick wall phase MON5, and the porous structure MON6, are the least favorable monolayers, but for different reasons. In MON1 each molecule is connected only to three neighbors via rather weak D2 connection, In MON3 and MON4, half of the molecules have weak four connections, and the other half of the molecules have only two of them. In MON5 each molecule has four neighbors; however, the dimer connections between them are weak (these are D1, Table 1). Finally, in MON6 each molecule only has three connections including one strong and two weak ones.

So, our theoretical method thus yielded six different phases, with three of them (canted MON8, waveform MON7, and domino MON2) being particularly stable. Only a single monolayer (the canted structure MON8) has so far been observed experimentally.[8,29,30] In this work we reported above the

PTCDI Molecules on the Au(111) Surface

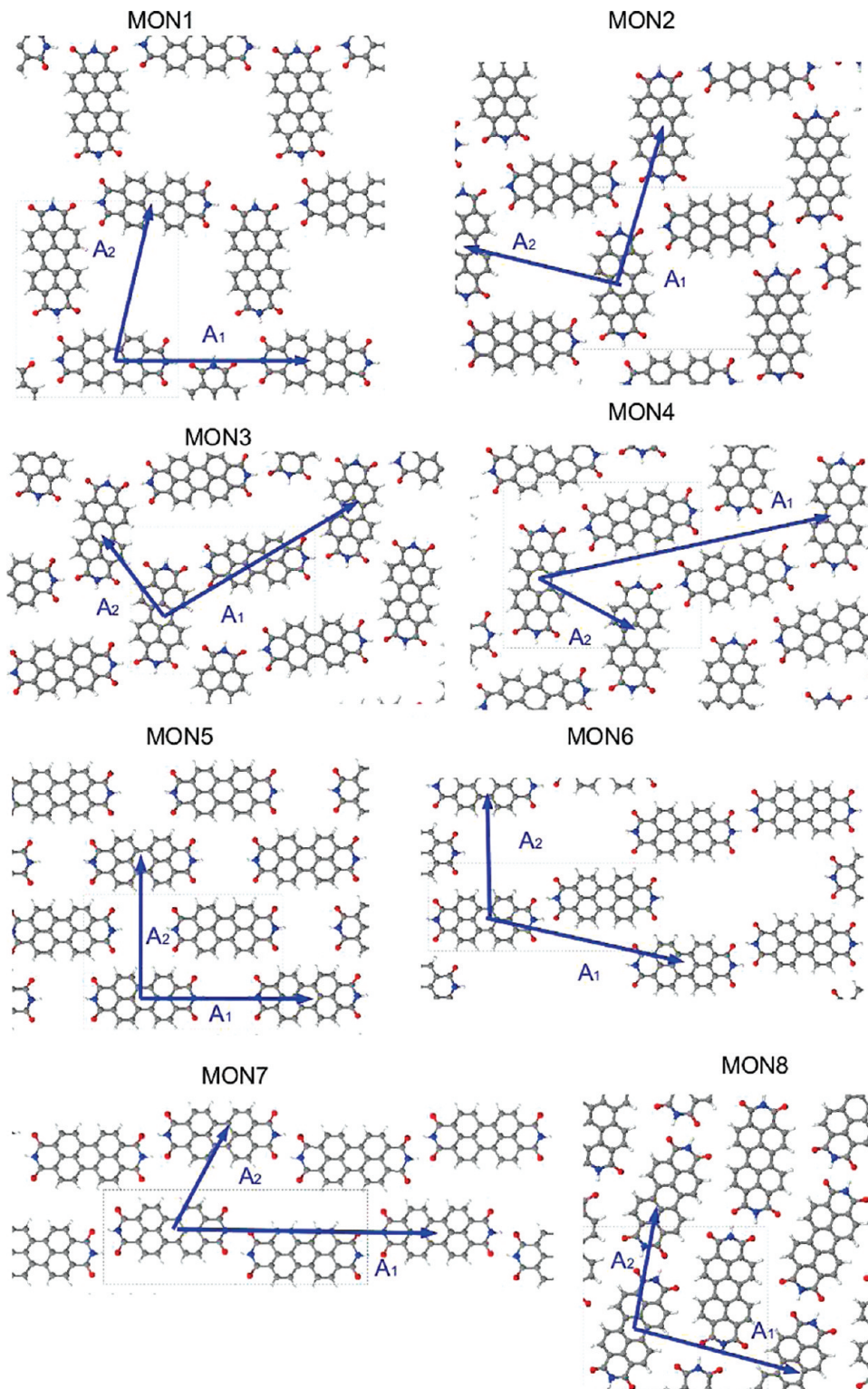*J. Phys. Chem. C, Vol. 113, No. 52, 2009* **21845**

Figure 5. DFT relaxed geometries of the selected eight prototype PTCDI monolayers. Lattice vectors as well as the unit cells are indicated. In the cases of MON5 and MON7 structures, based on true primitive cells with one molecule, the lattice vectors shown correspond to supercells containing two molecules.

experimental observations of two more structures, the domino and brick wall phases, both predicted correctly by our theoretical approach.

In Table 6 we compare the experimental geometries for various phases with those calculated above in the gas phase. In the canted structure, one can see that the canting angle β and the distance between molecules along the F4a row do not depend

significantly on the substrate (surprisingly, even in the case of a not-so-flat Au(11,12,12) surface) and are similar to our data calculated in the gas phase. However, other characteristics of the monolayer associated with the relative position of the rows with respect to each other (A_1 and the angle γ), may depend noticeably on the substrate and the preparation conditions (compare the Au(111) data of this work and of ref 30, although

TABLE 4: Evaluated and Calculated Stabilization Energies (in eV) for PTCDI Monolayers Shown in Figure 5[a]

phase	domino		herringbone		brick wall	porous	waveform	canted
index	MON1	MON2	MON3	MON4	MON5	MON6	MON7	MON8
E_{stab} (eval.)	−0.72	−0.96	−0.63	−0.72	−0.60	−0.80	−1.30	−1.55
E_{stab} (calc.)	−0.89	−1.12	−0.97	−0.91	−0.85	−0.99	−1.38	−1.67
E_{BSSE}	0.43	0.57	0.43	0.49	0.48	0.40	0.46	0.67

[a] The BSSE correction is also shown in each case. For the ease of comparison, energies for the MON5 and MON7 structures refer to the supercell containing two molecules.

TABLE 5: Lengths of Lattice Vectors (in Å) and the Angle between Them (in deg) for the Eight Selected PTCDI Monolayers[a]

phase	domino		herringbone		brick wall	porous	waveform	canted
index	MON1	MON2	MON3	MON4	MON5	MON6	MON7	MON8
A_1	22.25	18.0	26.11	26.12	18.84	24.3	28.63	17.45
A_2	17.92	18.01	12.05	12.23	15.86	15.9	11.62	14.51
γ	75.3	90.1	96.2	62.0	90.0	76.9	62.9	91.4

[a] For the ease of comparison, the lattice vectors of the MON5 and MON7 structures correspond to a supercell containing two molecules in agreement with Figure 5.
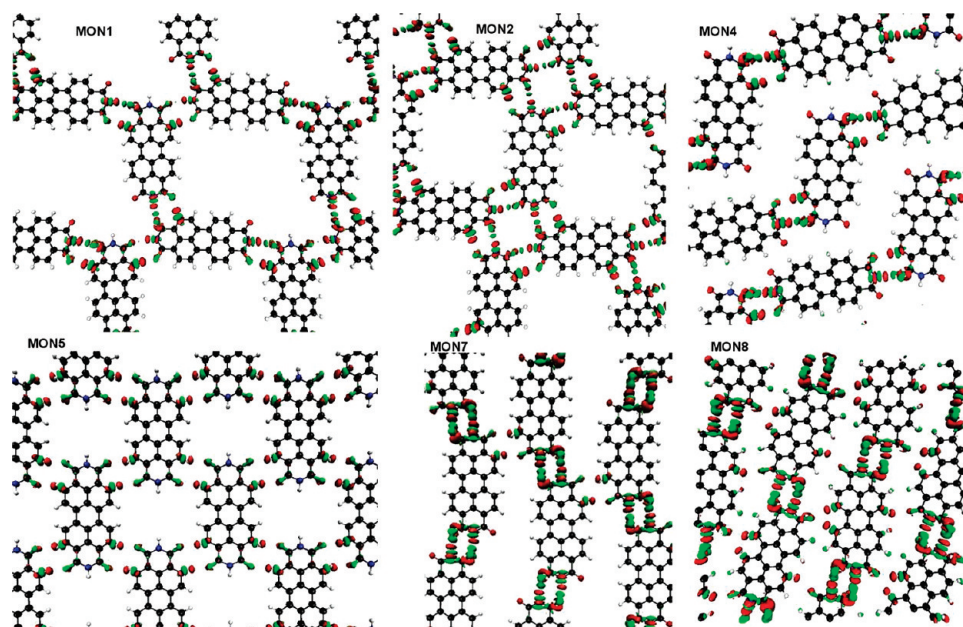

Figure 6. Electron density difference plots corresponding to ±0.01 electrons/Å^3 of some of the PTCDI monolayers. The green surface corresponds to the regions of positive electron difference (excess), and the red areas correspond to the regions of negative electrons density difference (depletion).

TABLE 6: Lengths (in Å) of the Two Lattice Vectors and the Angle γ (in deg) between Them for the Three Experimentally Observed PTCDI Phases[a]

phase	canted				brick wall			domino	
surface	Au(11,12,12)	Ag/Si(111)	Au(111)	DFT	NaCl(001)	Au(111)	DFT	Au(111)	DFT
reference	29	8	30	this work	28	this work		this work	
A_1	−	−	19.8	16.7	17.45	15.3	18.7	18.84	17.9	18.0
A_2	14.2	14.6	14.5	13.8	14.51	16.1	17.0	15.86	17.0	18.01
γ	−	−	105	100	91.4	90	90	90	95	90.1
β	11.0	−	12	12	11.5	−	−	−	−	−

[a] β is the canted angle along the F4a type rows (in deg) in the canted structure. The "DFT" columns correspond to our DFT gas-phase calculations, while all other columns correspond to experimental measurements.

the experimental data on these are only fully available for the Au(111) surface. This behavior is explained by extremely strong interaction between molecules along the F4a row as compared with their rather weak interaction between the rows, as noted above. Concerning the brick wall phase, the lattice vector A_2 is close for the both surfaces and for the gas-phase calculation;

however, the other lattice vector, A_1, which corresponds to the distance between rows of molecules, varies significantly depending on the particular surface or the absence of such.

The agreement between the gas-phase calculations and the observed structures on gold for the brick wall and domino phases is much better: we observe very close unit cells in each case.

This is due to more homogeneous distribution of interaction between the molecules as evidenced from Figure 6.

V. Conclusions

In this paper, using STM and a theoretical method, we have studied periodic assemblies which PTCDI molecules may form on the Au(111) surface. Previously only the canted and brick wall structures had been reported in the literature, of which one (the brick wall) had only been seen on a single substrate. One more structure, the domino phase, was observed and reported here for the first time.

To understand these findings, we followed a systematic theoretical approach in constructing 1D and 2D planar periodic PTCDI assemblies. Our method is based on predicting all possible structures in the gas phase by identifying and then utilizing all dimer connections between the molecules. In this way a variety of monolayers was built, which were then split into eight families of similar structures. After choosing a representative from every family, we proceeded further and relaxed the selected structures using an ab initio method. In this way eight possible structures have been predicted which represent six phases: domino, herringbone, brick wall, porous, waveform, and canted. The canted, waveform, and domino phases were found to be the most energetically favorable. The geometrical characteristics of the canted, brick wall, and domino phases calculated in the gas phase match very closely those observed experimentally by the STM method on the Au(111) surface in this work.

Separating all the structures into distinct families of structures and then into phases has a greater significance then simply to reduce the computational effort. The important point we can make here is that, due to limited resolution of the present scanning probe methods, atomistically different structures belonging to the *same* family are expected to appear in the STM images indistinguishable. Therefore, only theoretical calculations may predict the exact arrangements of the molecules on the surface in some cases.

Note that our theoretical analysis corresponds to zero temperature, and no account has been made of the entropic effects. The latter may be important in some cases to explain the preference of one structure over the other after, e.g., annealing.[50]

It is surprising, however, that the waveform phase, the second most favorable structure in the gas phase, has not been found in our STM images. It is not clear whether this can be attributed to the interaction with the surface. In our theoretical analysis the surface was not accounted for: if it had been, it could have made this particular structure less favorable. However, in view of the recent first principles detailed calculations[48] of a (quite similar) PTCDA molecule with the same gold surface in which the dispersion (van der Waals) interaction was accounted for within the newly developed vdW-DF functional,[51,52] this explanation seems to be unlikely since those calculations demonstrated that the molecule−surface interaction is rather flat laterally. However, given that the STM images show preferred orientations of the PTCDI networks with respect to the Au (111) surface, some degree of anisotropy of the substrate may influence the relative stability of the networks.[53] This remains an open problem. The importance of the molecule−surface interaction in relation to the gold and silver surfaces was discussed in refs 54 and 55.

There is also another point worth mentioning. In the case of the PTCDI molecules, one dimer connection is two times stronger than the best PTCDA dimer.[24] Nevertheless, the best 2D structure we find (the canted monolayer) has only slightly higher binding energy as compared with the best PTCDA monolayer,[24] which is unexpected. This result demonstrates the importance of other dimer connections involved in the binding of the monolayer: sometimes, in order to accommodate the strong bondings, weak connections must also be used, and this may reduce the overall stability of the assembly.

Our systematic method of constructing all possible supramolecular assemblies has been already applied to a wide variety of planar molecules capable of forming hydrogen bonding with each other, including DNA bases,[34,43,50,56−62] melamine,[35,44] PTCDA,[24] and PTCDI, considered here. We hope that this method will be found useful in predicting possible assemblies of other molecules as well.

References and Notes

(1) Theobald, J. A.; Oxtoby, N. S.; Phillips, M. A.; Champness, N. R.; Beton, P. H. *Nature* **2003**, *424*, 1029–1031.

(2) Madueno, R.; Raisanen, M. T.; Silien, C.; Buck, M. *Nature* **2008**, *454*, 618–621.

(3) Staniec, P. A.; Perdigão, L. M. A.; Rogers, B. L.; Champness, N. R.; Beton, P. H. *J. Phys. Chem. C* **2007**, *111*, 886–893.

(4) Silly, F.; Shaw, A. Q.; Porfyrakis, K.; Briggs, G. A. D.; Castell, M. R. *Appl. Phys. Lett.* **2007**, *91* (1−3), 253109.

(5) Charra, F.; Cousty, J. *Phys. Rev. Lett.* **1998**, *80*, 1682–1685.

(6) Viswanathan, R.; Zasadzinski, J. A.; Schwartz, D. K. *Nature* **1994**, *368*, 440–443.

(7) Rosei, F. *Prog. Surf. Sci.* **2003**, *71*, 95–146.

(8) Swarbrick, J. C.; et al. *J. Phys. Chem. B* **2005**, *109*, 12167–12174.

(9) Swarbrick, J. C.; Rogers, B. L.; Champness, N. R.; Beton, P. H. *J. Phys. Chem. B* **2006**, *110*, 6110–6114.

(10) Ma, J. *J. Phys. Chem. B* **2006**, *110*, 12539–12210.

(11) Ludwig, C.; Gompf, B.; Petersen, J.; Strohmaier, R.; Eisenmenger, W. *Z. Phys. B* **1994**, *93*, 365–373.

(12) Kilian, L. *Phys. Rev. Lett.* **2008**, *100*, 136103.

(13) Chinzhov, I.; Kahn, A.; Scoles, G. *J. Cryst. Growth* **2000**, *208*, 449–458.

(14) Mannsfeld, S.; Toerker, M.; Schmitz-Hubsch, T.; Sellam, F.; Fritz, T.; Leo, K. *Org. Electron.* **2001**, *2*, 121–134.

(15) Nicoara, N.; Roman, E.; Gomez-Rodriguez, J.; Martin-Gago, J.; Mendez, J. *Org. Electron.* **2006**, *7*, 287–294.

(16) Kunstmann, T. *Phys. Rev. B* **2005**, *71*, 121403.

(17) Fendrich, T.; Kunstmann, M.; Paulkowski, D.; Moller, R. *Nanotechnology* **2007**, *18*, 084004.

(18) Glockler, K.; et al. *Surf. Sci.* **1998**, *405*, 1–20.

(19) Wanger, T.; Bannani, A.; Bobisch, C.; Karacuban, H.; Moller, R. *J. Phys.: Condens. Matter* **2007**, *19*, 056009.

(20) Silly, F.; et al. *Phys. Rev. B* **2008**, *77* (1−4), 201408.

(21) Kröger, J.; Jensen, H.; Berndt, R.; Rurali, R.; Lorente, N. *Chem. Phys. Lett.* **2007**, *438*, 249–253.

(22) Gabriel, M.; Stöhr, M.; Möller, R. *Appl. Phys. A* **2002**, *74*, 303–305.

(23) Lauffer, P.; Emtsev, K.; Graupner, R.; Seyller, T.; Ley, L. *Phys. Status Solidi* **2008**, *245*, 2064–2067.

(24) Mura, M.; Silly, F.; Kantorovich, L. In preparation.

(25) Umbach, E.; Seidel, C.; Taborski, J.; Li, R.; Soukopp, A. *Phys. Status Solidi B* **1995**, *192*, 389–406.

(26) Aït-Mansour, K.; et al. *J. Phys. Chem. C* **2009**, *113*, 8407–8411.

(27) Guillermet, O.; Glachant, A.; Hoarau, J. Y.; Mossoyan, J. C.; Mossoyan, M. *Surf. Sci.* **2004**, *548*, 129–137.

(28) Topple, J. M.; Burke, S. A.; Fostner, S.; Grütter, P. *Phys. Rev. B* **2009**, *79*, 205414.

(29) Cañas, M. E.; et al. *Angew. Chem., Int. Ed.* **2007**, *46*, 1814–1818.

(30) Silly, F.; Shaw, A. Q.; Castell, M. R.; Briggs, G. A. D. *Chem. Commun.* **2008**, 1907–1909.

(31) Nowakowski, R.; Seidel, C.; Fuchs, H. *Surf. Sci.* **2004**, *562*, 53–64.

(32) Binnig, G.; Rohrer, H.; Gerber, C.; Weibel, E. *Phys. Rev. Lett.* **1983**, *50*, 120–123.

(33) Binnig, G.; Rohrer, H. *Rev. Mod. Phys.* **1987**, *59*, 615–625.

(34) Kelly, R. E. A.; Kantorovich, L. N. *J. Mater. Chem.* **2006**, *16*, 1984–1905.

(35) Mura, M.; Martsinovich, N.; Kantorovich, L. *Nanotechnology* **2008**, *46*, 465704.

(36) Silly, F. *J. Microsc. Oxford* **2009**, *236*, 211−218.

(37) Sanchez-Portal, D.; Ordejon, P.; Artacho, E.; Soler, J. *Int. J. Quantum Chem.* **1997**, *65*, 453–461.

(38) Soler, J. M.; et al. *J. Phys.: Condens. Matter* **2002**, *14*, 2745–2779.

(39) Troullier, N.; Martins, J. L. *Phys. Rev. B* **1991**, *43*, 1993–2006.

(40) Kleinman, L. *Phys. Rev. B* **1980**, *21*, 2630–2631.

(41) Perdew, J. P.; Burke, K.; Ernzerhof, M. *Phys. Rev. Lett.* **1996**, *77*, 3865–3868.

(42) Kelly, R. E. A.; Lee, Y.; Kantorovich, L. N. *J. Phys. Chem. B* **2005**, *109*, 22045–22052.

(43) Kelly, R. E. A.; et al. *Small* **2008**, *4*, 1494–1500.

(44) Silly, F.; et al. *J. Phys. Chem. C* **2008**, *112*, 11476–11480.

(45) Boys, S. F.; Bernardi, F. *Mol. Phys.* **1970**, *19*, 553.

(46) Kelly, R. E. A.; Lee, Y.; Kantorovich, L. N. *J. Phys. Chem. B* **2005**, *109*, 11933–11939.

(47) Kelly, R. E. A.; Lee, Y.; Kantorovich, L. N. *J. Phys. Chem. B* **2006**, *110*, 2249–2255.

(48) Mura, M.; Gulans, A.; Thonhauser, T.; Kantorovich, L. *Phys. Chem. Chem. Phys.* Submitted.

(49) Perdigao, L.; et al. *Chem.−Eur. J.* **2008**, *14*, 7600–7607.

(50) Xu, W.; et al. *Small* **2009**, *5*, 1952–1956.

(51) Dion, M.; Rydberg, H.; Schröder, E.; Langreth, D. C.; Lundqvist, B. I. *Phys. Rev. Lett.* **2004**, *92* (1−4), 246401.

(52) Gulans, A. *Phys. Rev. B* **2009**, *79*, 201105(R).

(53) Silly, F.; Shaw, A. Q.; Briggs, G. A. D.; Castell, M. R. *Appl. Phys. Lett.* **2008**, *92* (1−3), 023102.

(54) Henze, S. K. M.; Bauer, O.; Lee, T.-L.; Sokolowski, M.; Tautz, F. S. *Surf. Sci.* **2007**, *601*, 1566–1573.

(55) Eremtchenko, M.; Schaefer, J. A.; Tautz, F. S. *Nature* **2003**, *425*, 602–605.

(56) Lukas, M.; et al. *J. Chem. Phys.* **2009**, *130* (1−9), 024705.

(57) Mamdouh, W.; Kelly, R. E. A.; Dong, M.; Kantorovich, L. N.; Besenbacher, F. *J. Am. Chem. Soc.* **2008**, *130*, 695–702.

(58) Xu, W.; et al. *Small* **2007**, *3*, 2011–2014.

(59) Otero, R.; et al. *Angew. Chem., Int. Ed.* **2008**, *47*, 9673–9676.

(60) Mamdouh, W.; Dong, M.; Kelly, R. E. A.; Kantorovich, L. N.; Besenbacher, F. *J. Phys. Chem. B* **2007**, *111*, 12048–12052.

(61) Perdigão, L. M. A.; et al. *Phys. Rev. B* **2006**, *73* (1−6), 195423.

(62) Otero, R.; et al. *Science* **2008**, *319*, 312–315.